

Effects of upper disc boundary conditions on the linear Rossby wave instability

Min-Kai Lin ^{*}

Canadian Institute for Theoretical Astrophysics, 60 St. George Street, Toronto, ON, M5S 3H8, Canada

19 July 2018

ABSTRACT

The linear Rossby wave instability (RWI) in global, three-dimensional (3D) polytropic discs is revisited with a much simpler numerical method than that previously employed by the author. The governing partial differential equation is solved with finite-differences in the radial direction and spectral collocation in the vertical direction. RWI modes are calculated subject to different upper disc boundary conditions. These include free surface, solid boundaries and variable vertical domain size. Boundary conditions that oppose vertical motion increases the instability growth rate by a few per cent. The magnitude of vertical flow throughout the fluid column can be affected but the overall flow pattern is qualitatively unchanged. Numerical results support the notion that the RWI is intrinsically two-dimensional. This implies that inconsistent upper disc boundary conditions, such as vanishing enthalpy perturbation, may inhibit the RWI in 3D.

1 INTRODUCTION

The Rossby wave instability (RWI, Lovelace et al. 1999; Li et al. 2000) is the thin-disc analog of the Papaloizou-Pringle instability in thick tori (Papaloizou & Pringle 1984, 1985, 1987). The RWI is a shear instability associated with extrema in the potential vorticity profile of a disc. Its occurrence in radially structured protoplanetary discs, leading to vortex formation (Li et al. 2001), can transport angular momentum, assist planet formation (Lyra et al. 2008, 2009) and affect planetary migration (Li et al. 2009; Lin & Papaloizou 2010).

The RWI was originally described in two-dimensional (2D) discs. Recent works show that it can operate in three-dimensional (3D) geometry (Umurhan 2010; Meheut et al. 2010, 2012a,b; Lin 2012a). In these calculations the perturbation extends vertically through the disc, but the effect of conditions at the disc surface was not investigated. This might be a relevant issue for the RWI to develop in non-magnetized regions of protoplanetary discs (Lyra & Mac Low 2012). In the layered accretion scenario, this ‘dead zone’ is overlaid by an actively accreting layer (Gammie 1996; Okuzumi & Hirose 2011; Martin et al. 2012). A first step towards revealing vertical boundary effects on the 3D RWI is to calculate it subject to different upper disc boundary conditions.

Previous linear RWI simulations assume the zero-density surface as the upper disc boundary. When the density stratification has the appropriate functional form, regularity conditions enable the vertical dependence of perturbations to be expressed in terms of classic orthogonal polynomials (Papaloizou & Pringle 1985; Takeuchi & Miyama

1998). The linear problem becomes a set of ordinary differential equations (ODE), but these ODEs can be complicated. Furthermore, this approach does not permit boundary conditions at other heights to be imposed (Lin 2012a, hereafter L12).

The purpose of this work is to address the above caveat of L12. An alternative numerical method is applied to the linear problem so that effects of upper disc boundary conditions can be explored through simple numerical experiments. This paper is organized as follows. §2 defines the equilibrium and perturbed disc. §3 gives a step-by-step description to convert the problem into a single matrix equation. Solutions are presented in §4 and discussed in §5.

2 MODEL AND GOVERNING EQUATIONS

The system is a geometrically thin, non-self-gravitating, inviscid fluid disc orbiting a central star of mass M_* . The disc is governed by the Euler equations in (r, ϕ, z) cylindrical co-ordinates centered on the star. Units such that the gravitational constant $G = M_* = 1$ are adopted. A polytropic equation of state is assumed, so that the pressure P is related to the density ρ by $P = K\rho^{1+1/n}$, where n is the polytropic index and K is a constant.

Details of the equilibrium disc are given in L12. The unperturbed disc is steady and axisymmetric with surface density profile in the form $\Sigma \propto r^{-\alpha}B(r)$, where $B(r)$ describes a Gaussian bump centered at $r = r_0$ with amplitude A and width Δr . The density is $\rho(r, z) = \rho_0(r)[1 - z^2/H^2(r)]^n$, where ρ_0 is the midplane density and $H(r)$ is the disc thickness. The unperturbed velocity field is

arXiv:1210.6656v1 [astro-ph.EP] 24 Oct 2012

$(v_r, v_\phi, v_z) = (0, r\Omega, 0)$ where $\Omega(r)$ is the angular velocity, and $\Omega \simeq \Omega_k \equiv \sqrt{GM_*/r^3}$. Fiducial parameter values are: $\alpha = 0.5$, $r_0 = 1$, $A = 1.4$, $\Delta r = 0.05r_0$ and $H(r_0) = 0.14r_0$.

Eulerian perturbations to the above equilibrium in the form $\text{Re}[\delta\rho(r, z) \exp(i(\sigma t + m\phi))]$ are considered. $\sigma = -(\omega + i\gamma)$ is a complex eigenfrequency and m is a positive integer. γ and $-\omega$ are the mode growth rate and real frequency, respectively. The linearized fluid equations yield the following partial differential equation (PDE):

$$r\delta\rho = \frac{\partial}{\partial r} \left(\frac{r\rho}{D} \frac{\partial W}{\partial r} \right) + \frac{2mW}{\bar{\sigma}} \frac{\partial}{\partial r} \left(\frac{\rho\Omega}{D} \right) - \left(\frac{m^2\rho}{rD} \right) W - \frac{r}{\bar{\sigma}^2} \frac{\partial}{\partial z} \left(\rho \frac{\partial W}{\partial z} \right) \quad (1)$$

(L12), where $W \equiv \delta P/\rho$ is the enthalpy perturbation and $D \equiv \kappa^2 - \bar{\sigma}^2$; where $\kappa^2 \equiv r^{-3} d(r^4\Omega^2)/dr$ is the square of the epicyclic frequency and $\bar{\sigma} = \sigma + m\Omega$ is the shifted frequency. The RWI is associated with an extremum in potential vorticity ($\eta \equiv \kappa^2/2\Omega\Sigma$, Lovelace et al. 1999). In the above setup $\min(\eta)$ occurs near r_0 , so that $\bar{\sigma}(r_0) \sim 0$. The aim is to solve Eq. 1 as a PDE eigenvalue problem with various boundary conditions applied at $z/H = Z_s$.

For simplicity Z_s is assumed constant, but extension to $Z_s = Z_s(r)$ is straight forward provided that $Z_s(r) \neq 0$ (in which case transformation to polar-like coordinates is needed, see Papaloizou & Pringle 1984).

2.1 Vertical boundary conditions

The enthalpy perturbation is assumed to be symmetric about the midplane, since even modes have been found to dominate in nonlinear simulations (Meheut et al. 2010). The upper disc boundary is set to $Z_s < 1$, thus avoiding the disc surface where the PDE becomes singular. The following upper boundary conditions (BC) were found to permit the RWI.

‘Open’ boundary. The Lagrangian pressure perturbation vanishes at Z_s :

$$\Delta P \equiv \delta P + \boldsymbol{\xi} \cdot \nabla P = 0 \quad (2)$$

where $\boldsymbol{\xi}$ is the Lagrangian displacement. If Z_s is unity then this is the usual condition for polytropes with vanishing pressure at its surface (which is satisfied automatically for regular solutions).

‘Solid’ boundaries. At Z_s the meridional velocity perturbation satisfies

$$\delta v_z = \nu \delta v_r, \quad (3)$$

where $\nu = \nu(r)$ is a real function. Choosing $\nu = Z_s dH/dr$ corresponds to zero velocity perpendicular to the upper disc boundary ($\delta v_\perp = 0$). This applies to an impermeable surface. The simpler choice $\nu \equiv 0$ corresponds to zero vertical velocity ($\delta v_z = 0$). This might apply, for example, when vertical velocities are strongly damped above Z_s . In practice, the two conditions are similar because $|\nu| \ll 1$ for a thin disc.

3 NUMERICAL METHOD

It is convenient to adopt the co-ordinate system $(R, Z) \equiv (r, z/H)$ so the computational domain is rectangular for con-

stant Z_s . Then the governing equation becomes

$$0 = \mathcal{A} \frac{\partial^2 W}{\partial R^2} + \mathcal{B} \frac{\partial^2 W}{\partial Z \partial R} + \mathcal{C} \frac{\partial^2 W}{\partial Z^2} + \mathcal{D} \frac{\partial W}{\partial R} + \mathcal{E} \frac{\partial W}{\partial Z} + \mathcal{F} W, \quad (4)$$

$$\mathcal{A} = (1 - Z^2)R^2, \quad (5)$$

$$\mathcal{B} = -2Z(1 - Z^2)R^2 \frac{H'}{H}, \quad (6)$$

$$\mathcal{C} = Z^2(1 - Z^2)R^2 \left(\frac{H'}{H} \right)^2 - \frac{R^2 D(1 - Z^2)}{\bar{\sigma}^2 H^2}, \quad (7)$$

$$\mathcal{D} = \left[\ln \left(\frac{\rho_0 R}{D} \right) \right]' (1 - Z^2)R^2 + 2nZ^2 R^2 \frac{H'}{H}, \quad (8)$$

$$\mathcal{E} = 2nZ \frac{R^2 D}{\bar{\sigma}^2 H^2} + ZR^2 \left(\frac{H'}{H} \right)^2 [1 - (2n + 1)Z^2] - Z(1 - Z^2)R^2 \left\{ \left(\frac{H'}{H} \right)' + \left(\frac{H'}{H} \right) \left[\ln \left(\frac{\rho_0 R}{D} \right) \right]' \right\}, \quad (9)$$

$$\mathcal{F} = \frac{2mR\Omega}{\bar{\sigma}} \left[\ln \left(\frac{\rho_0 \Omega}{D} \right) \right]' (1 - Z^2) + 2nZ^2 \left(\frac{2mR\Omega H'}{\bar{\sigma} H} \right) - m^2(1 - Z^2) - \frac{nD\rho_0^{-1/n} R^2}{K(1 + n)}, \quad (10)$$

and primes denote differentiation with respect to the argument.

To construct a numerical scheme, the radial co-ordinate is discretized into N_R grid points uniformly spaced by ΔR . Let R_i denote the radial co-ordinate of the i^{th} grid point, define $W_i(Z)$ as the solution along the vertical line $R = R_i$ and approximate it with a linear combination of basis functions,

$$W_i(Z) \equiv W(R_i, Z) = \sum_{k=1}^{N_Z} a_{ki} \psi_k(Z/Z_s), \quad (11)$$

for $1 \leq i \leq N_R$, with $\psi_k = T_{2(k-1)}$, where T_l is a Chebyshev polynomial of the first kind of order l (Abramowitz & Stegun 1965). The number of basis functions is N_Z and $l_{\text{max}} = 2(N_Z - 1)$ is the highest polynomial order.

The pseudo-spectral coefficients a_{ki} are obtained by demanding the governing PDE, Eq. 4, to be satisfied at vertical grid points Z_j along each line, where

$$Z_j = -Z_s \cos \left[\frac{(j-1 + l_{\text{max}}/2)\pi}{l_{\text{max}}} \right] \quad 1 \leq j \leq N_Z \quad (12)$$

This is a standard choice for collocation points in pseudo-spectral methods with Chebyshev polynomials (Boyd 2001). Note that only the upper half plane ($z \geq 0$) is covered, by the assumption of symmetry.

The next step is to insert Eq. 11 into Eq. 4 and evaluate the governing PDE at each (R_i, Z_j) . Radial derivatives are approximated with central differences while vertical derivatives are computed exactly. At each grid point the result

is

$$\begin{aligned}
 0 = & \sum_{k=1}^{N_Z} a_{ki} \times \left[\left(\mathcal{F}_{ij} - \frac{2\mathcal{A}_{ij}}{\Delta R^2} \right) \psi_{kj} + \mathcal{E}_{ij} \frac{\psi'_{kj}}{Z_s} + \mathcal{C}_{ij} \frac{\psi''_{kj}}{Z_s^2} \right] \\
 & + \sum_{k=1}^{N_Z} a_{k,i-1} \times \left[\left(\frac{\mathcal{A}_{ij}}{\Delta R^2} - \frac{\mathcal{D}_{ij}}{2\Delta R} \right) \psi_{kj} - \frac{\mathcal{B}_{ij}}{2\Delta R} \frac{\psi'_{kj}}{Z_s} \right] \\
 & + \sum_{k=1}^{N_Z} a_{k,i+1} \times \left[\left(\frac{\mathcal{A}_{ij}}{\Delta R^2} + \frac{\mathcal{D}_{ij}}{2\Delta R} \right) \psi_{kj} + \frac{\mathcal{B}_{ij}}{2\Delta R} \frac{\psi'_{kj}}{Z_s} \right], \quad (13)
 \end{aligned}$$

where $\mathcal{A}_{ij} = \mathcal{A}(R_i, Z_j)$ and similarly for other PDE coefficients, and $\psi_{kj} \equiv \psi_k(Z_j/Z_s)$. Eq. 13 can be written in matrix notation:

$$\mathbf{V}^{(i)} \mathbf{a}^{(i)} + \mathbf{V}_-^{(i)} \mathbf{a}^{(i-1)} + \mathbf{V}_+^{(i)} \mathbf{a}^{(i+1)} = \mathbf{0}. \quad (14)$$

The operators $\mathbf{V}^{(i)}$ and $\mathbf{V}_\pm^{(i)}$ are $N_Z \times N_Z$ matrices and the column vector $\mathbf{a}^{(i)}$ consists of the N_Z pseudo-spectral coefficients associated with the i^{th} line. $\mathbf{V}_\pm^{(i)}$ represent coupling to adjacent lines. The matrix elements can be read off Eq. 13.

For simplicity, $\partial_R W = 0$ is set at radial boundaries¹. This is achieved implicitly by setting $a_{k,i-1} = a_{k,i+1}$ for $i = 1, N_R$. $\mathbf{V}_+^{(1)}$ and $\mathbf{V}_-^{(N_R)}$ are modified accordingly. At Z_s , the governing equation is replaced by upper disc boundary conditions listed in §2.1. This corresponds to modifying the PDE coefficients and the matrix elements for $j = N_Z$.

There are N_R lines in total, so the entire system of equations is

$$\mathbf{M} \mathbf{a} = \mathbf{0}, \quad (15)$$

where \mathbf{M} is a $(N_R N_Z) \times (N_R N_Z)$ block tridiagonal matrix and \mathbf{a} is a column vector of length $N_R N_Z$, representing the linear operators and the a_{ki} , respectively.

The discretized problem, Eq. 15, is a set of linear homogeneous equations. A solution method is described in L12. The eigenfrequency σ is varied, using Newton-Raphson iteration, until the matrix \mathbf{M} becomes singular. Only solutions where the reciprocal condition number of \mathbf{M} is zero at machine precision are accepted. LAPACK was used for the matrix operations, which also yield \mathbf{a} up to an arbitrary normalization.

4 LINEAR SIMULATIONS

The computational domain is $R \in [0.4, 1.6]r_0$ and $Z_s = 0.9$ or $Z_s = 0.45$. The default polytropic index is $n = 1.5$ but cases with $n = 0.7, 2.5$ are also presented. Linear modes with azimuthal wavenumber $m = 3$ are considered.

The fiducial case below employed a trial frequency $\sigma = -(0.994m + 0.107i)\Omega_0$ where $\Omega_0 \equiv \Omega(r_0)$. This was the solution found in L12. Eigenfrequencies for other parameter values may be found by varying those parameters slowly away from fiducial values. The numerical grid is $(N_R, N_Z) = (384, 8)$, which corresponds to $l_{\text{max}} = 14$ (cf. $l_{\text{max}} = 6$ in L12).

Table 1 summarizes the calculations. The last column,

Table 1. Summary of linear simulations. The azimuthal wavenumber is $m = 3$ for all cases.

Case	n	Z_s	BC	$\omega/m\Omega_0$	γ/Ω_0	$\langle \theta_m \rangle$
1a	1.5	0.90	$\Delta P = 0$	0.9941	0.1074	0.31
1b	1.5	0.45	$\Delta P = 0$	0.9997	0.0889	0.36
2a	1.5	0.90	$\delta v_\perp = 0$	0.9940	0.1091	0.26
2b	1.5	0.45	$\delta v_\perp = 0$	0.9939	0.1174	0.06
3a	1.5	0.90	$\delta v_z = 0$	0.9945	0.1086	0.26
3b	1.5	0.45	$\delta v_z = 0$	0.9973	0.1143	0.06
4a	0.7	0.90	$\Delta P = 0$	0.9959	0.1976	0.34
4b	0.7	0.90	$\delta v_z = 0$	0.9968	0.2034	0.22
5a	2.5	0.90	$\Delta P = 0$	0.9926	0.0359	0.39
5b	2.5	0.90	$\delta v_z = 0$	0.9927	0.0361	0.38

$\langle \theta_m \rangle$, is a measure of three-dimensionality of the flow near r_0 . θ_m is defined by

$$\theta_m^2(r, z) \equiv \tilde{v}_z^2 / (\tilde{v}_z^2 + \tilde{v}_r^2), \quad (16)$$

where $\tilde{v}_{r,z} \equiv \text{Re}[\delta v_{r,z} W^*(r_0, 0)] / |W(r_0, 0)|$ is the real velocity perturbation at an azimuth close to a local maximum in midplane enthalpy perturbation (hereafter the *vortex core*). $\langle \cdot \rangle$ denotes spatial averaging over $R \in [0.8, 1.2]r_0$ and $Z \in [0, Z_s]$.

4.1 Fiducial case

The numerical method is first tested against L12 with the open boundary (case 1a). Fig. 1 shows W at several heights and the perturbed real velocity field projected onto the (r, z) plane. $|W|$ has a weak vertical dependence in the co-rotation region $r \in [0.8, 1.2]r_0$. The enthalpy perturbation becomes increasingly three-dimensional away from r_0 . Near Z_s , the disturbance in the wave-region can reach amplitudes comparable to that near r_0 . This means the RWI becomes radially global at large heights.

The above result, considered as the intrinsic solution, is very similar to L12, including the growth rate and radially converging flow towards r_0 with upwards motion at the vortex core. This validates the choice of solution method.

4.2 Solid boundaries

Comparison of case 2a ($\delta v_\perp = 0$) and 3a ($\delta v_z = 0$) with the reference case above show that a solid boundary only has a minor effect on the instability growth rate. The perturbation for case 3a is plotted in Fig. 2.

In comparison with case 1a, the enthalpy perturbation in the co-rotation region is unaffected by solid boundaries. There is, however, a decrease in three-dimensionality as indicated by $\langle \theta_m \rangle$. This correlates with a slight increase in growth rate, suggesting that suppressing vertical motions favor instability.

A solid upper boundary causes the disturbance to become more two-dimensional in the wave-region. Compared to Fig. 1, for $r < 0.6r_0$ the amplitude of $W(r, 0.9H)$ has decreased while that for $W(r, 0)$ has increased. Consequently, the magnitude of the vertical flow is smaller in case 3a than in case 1a.

¹ The RWI typically has disturbance radially confined near r_0 and therefore insensitive to distant radial boundaries.

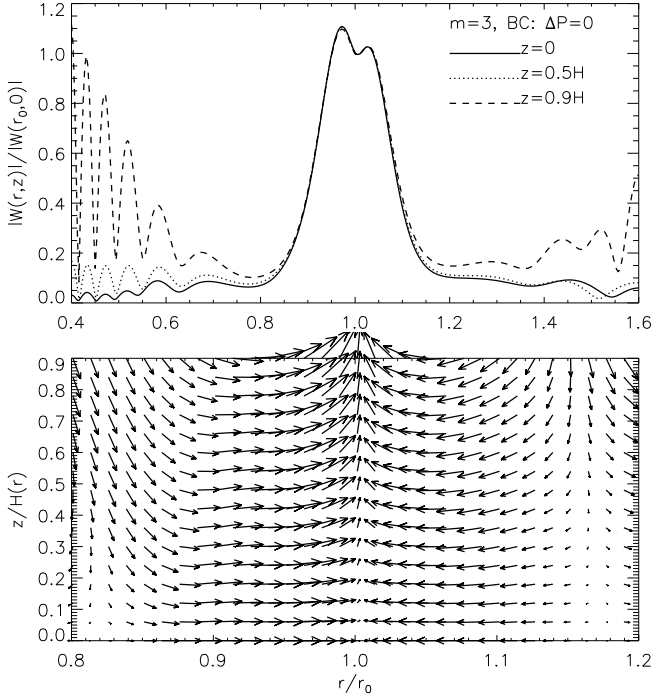


Figure 1. Reference case with $\Delta P = 0$ at Z_s . The normalized enthalpy perturbation, $|W(r, z)/W(r_0, 0)|$ (top), and the perturbed meridional velocity (bottom) are shown. The real velocity field is taken at the vortex core. Velocities are normalized so its magnitude can be compared to other cases.

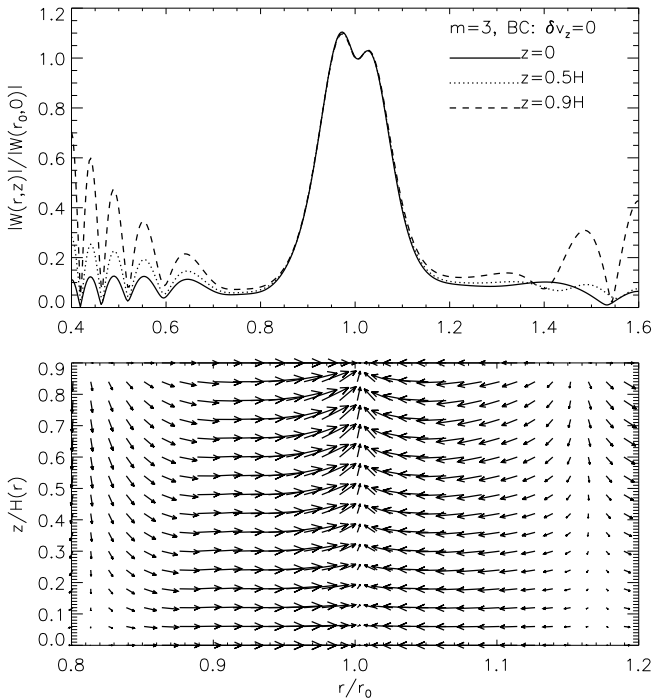


Figure 2. Same as Fig. 1 but with $\delta v_z = 0$ applied at Z_s .

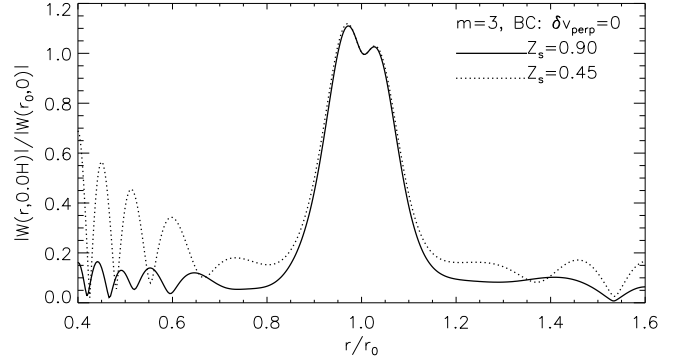


Figure 3. Midplane enthalpy perturbations subject to $\delta v_{\perp} = 0$ at two values of Z_s .

4.3 Effect of domain height

In case 2b and 3b the vertical domain is reduced from cases 2a and 3a, respectively. This increases the growth rate by $< 8\%$ but $\langle \theta_m \rangle$ is reduced by a factor of 3–4. When θ_m is averaged over $Z \in [0, 0.45]$, cases 2a and 3a have $\langle \theta_m \rangle = 0.19$. So the reduction in three-dimensionality with decreased Z_s is not simply due to averaging over a region closer to the midplane (towards which $\delta v_z \rightarrow 0$).

Fig. 3 compares $|W(r, 0)|$ between cases 2a and 2b. The co-rotation region is unchanged. (Note that $\delta v_z \propto \partial_z W / \bar{\sigma}$ and $|\bar{\sigma}(r_0)|/\Omega_0 \ll 1$, so a small difference in $\partial_z W$ between the two cases can still result in an appreciable difference in vertical velocity.) The perturbation magnitude in $r < 0.8$, $r > 1.2$ has noticeably increased with reduced disc thickness. In this sense the RWI has been made more radially global by restricting the fluid to a thinner slab.

Case 1b has $\Delta P = 0$ applied $Z_s = 0.45$. This corresponds to a situation where conditions above the upper boundary adjust according to the RWI in $Z < Z_s$, which is of course unrealistic. Nevertheless, it is interesting to note that the growth rate has decreased compared to case 1a, but as above this correlates with an increase in three-dimensionality.

4.4 Dependence on polytropic index

L12 found that the vertical flow in the vortex core increases in magnitude with decreasing polytropic index when other parameters are fixed. This is reflected in Fig. 4 when the open boundary is applied. As n is lowered from 2.5 to 0.7, the maximum vertical velocity increases by a factor of ~ 6 . For each n , a calculation with a solid boundary is also shown, for which the increase in vertical velocity is less significant (by a factor ~ 3).

Fig. 4 indicate upper disc boundary conditions are more important for smaller polytropic indices. The dotted curve for $n = 2.5$ only deviates from the solid curve in $Z \gtrsim 0.6$. For $n = 0.7$, forcing the flow to be horizontal at Z_s causes the disturbance to be more two-dimensional throughout the column of the fluid.

In previous studies with a vertically isothermal disc (equivalent to a polytrope with $n \rightarrow \infty$), the vortex core appears hydrostatic (Meheut et al. 2012b, L12). So for large n explicitly setting $\delta v_z = 0$ at Z_s makes little difference. Con-

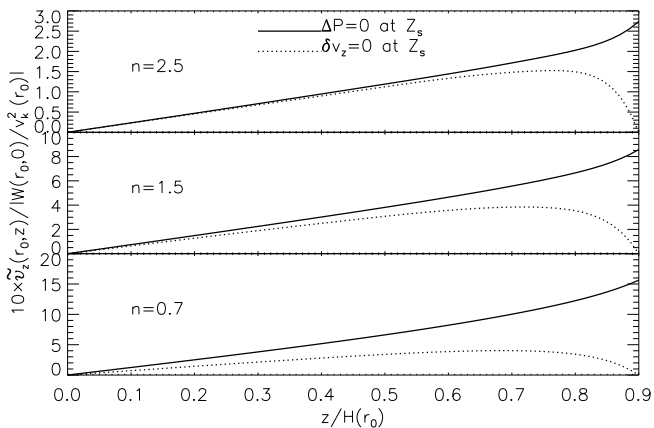


Figure 4. Normalized vertical velocity near a local maximum in midplane enthalpy perturbation for a range of polytropic indices n and upper disc boundary conditions. Here $v_k \equiv r\Omega_k$.

versely, as n is lowered the intrinsic solution acquires larger $|v_z|$ at the vortex core, so that the effect of forcing $\delta v_z \rightarrow 0$ at the upper boundary becomes global in the vertical direction.

Imagine setting up the RWI with $\Delta P = 0$ at Z_s , but during its development force $\delta v_z \rightarrow 0$ at Z_s . Suppose upper boundary effects are communicated through the fluid by sound waves. The sound-speed in a polytrope is $c_s \equiv \sqrt{dP/d\rho} = \Omega_k H(1 - Z^2)^{1/2} / \sqrt{2n}$, and the vertical sound-crossing time is $\tau_c \sim H/c_s \propto \sqrt{n}/\Omega_k$. In unit time, the change in boundary condition should affect the lower n polytrope deeper into the disc than higher n , as observed in Fig. 4. (This is also seen when the bump amplitude A for each n was adjusted to achieve equal growth rates.)

4.5 Other experiments

Additional calculations have been performed with a variable surface function $Z_s = Z_s(r)$. Examples include a surface of constant aspect-ratio (with $\delta v_\perp = 0$) and a surface of constant pressure (with $\Delta P = 0$). In this case a second co-ordinate transformation is required. Similar results to previous experiments were obtained, including the aforementioned trend of growth rate with respect to disc thickness. The RWI appears insensitive to the exact shape of the upper disc boundary as well.

5 DISCUSSION

Linear simulations of the RWI with different upper disc boundary conditions have been performed. Changing from a free surface to a solid boundary increase growth rates slightly. This is accompanied by a decrease in the three-dimensionality of the flow at the vortex core. Confining the fluid to a smaller vertical domain has the same effect. This suggests 3D effects are weakly stabilizing (Li et al. 2003). However, upper disc boundary conditions affect the vertical flow throughout the vertical extent of the vortex core. This effect is stronger for decreasing polytropic index n , which corresponds to decreasing compressibility.

The above results support previous interpretations that

the RWI is largely two-dimensional (Umurhan 2010; Lin 2012a). The linear growth rate and general flow pattern is insensitive to details of the upper disc boundary conditions, *provided it is consistent with the 2D solution*. A counter-example is vanishing enthalpy perturbation at the upper disc boundary². Indeed, in this case no RWI-like modes were found (i.e. modes with enthalpy disturbances radially confined to the bump). Inappropriate upper disc boundary conditions may suppress the RWI as seen in linear and nonlinear simulations performed to date (e.g. Meheut et al. 2012a).

Experimenting with different vertical boundary conditions, as done here, is only a crude way to mimic possible boundary effects in a protoplanetary disc. However, failure to find the RWI for some conditions imply that whether or not the RWI can develop in protoplanetary discs depends on the disc vertical structure, which can be complicated (Terquem 2008). Calculating the RWI for protoplanetary discs will ultimately require multi-layer fluid models (Umurhan 2012).

The solution method in this paper supersedes L12 for its simplicity and ability to admit different upper disc boundary conditions. Also, it does not rely on the functional form of the background stratification. In principle, it can be applied to non-barotropic perturbations since inclusion of the energy equation only changes the coefficients of the governing PDE. Assuming the RWI is not modified significantly, then this solution method should be suitable for discs with entropy gradients. This will be the subject of a follow-up paper (Lin 2012b, submitted).

REFERENCES

- Abramowitz M., Stegun I. A., 1965, Handbook of mathematical functions with formulas, graphs, and mathematical tables, Abramowitz, M. & Stegun, I. A., ed.
 Boyd J., 2001, Chebyshev and Fourier Spectral Methods, Dover books on mathematics. Dover Publications
 Gammie C. F., 1996, ApJ, 457, 355
 Li H., Colgate S. A., Wendroff B., Liska R., 2001, ApJ, 551, 874
 Li H., Finn J. M., Lovelace R. V. E., Colgate S. A., 2000, ApJ, 533, 1023
 Li H., Lubow S. H., Li S., Lin D. N. C., 2009, ApJL, 690, L52
 Li L.-X., Goodman J., Narayan R., 2003, ApJ, 593, 980
 Lin M.-K., 2012a, ApJ, 754, 21
 Lin M.-K., 2012b, ArXiv: 1209.0470
 Lin M.-K., Papaloizou J. C. B., 2010, MNRAS, 405, 1473
 Lovelace R. V. E., Li H., Colgate S. A., Nelson A. F., 1999, ApJ, 513, 805
 Lyra W., Johansen A., Klahr H., Piskunov N., 2008, A&A, 491, L41
 Lyra W., Johansen A., Zsom A., Klahr H., Piskunov N., 2009, A&A, 497, 869
 Lyra W., Mac Low M.-M., 2012, ApJ, 756, 62
 Martin R. G., Lubow S. H., Livio M., Pringle J. E., 2012, MNRAS, 420, 3139

² This can be satisfied by choosing the basis functions as $\psi_k = T_{2k} - T_0$.

- Meheut H., Casse F., Varniere P., Tagger M., 2010, *A&A*, 516, A31
- Meheut H., Keppens R., Casse F., Benz W., 2012a, *A&A*, 542, A9
- Meheut H., Yu C., Lai D., 2012b, *MNRAS*, 422, 2399
- Okuzumi S., Hirose S., 2011, *ApJ*, 742, 65
- Papaloizou J. C. B., Pringle J. E., 1984, *MNRAS*, 208, 721
- Papaloizou J. C. B., Pringle J. E., 1985, *MNRAS*, 213, 799
- Papaloizou J. C. B., Pringle J. E., 1987, *MNRAS*, 225, 267
- Takeuchi T., Miyama S. M., 1998, *PASJ*, , 50, 141
- Terquem C. E. J. M. L. J., 2008, *ApJ*, 689, 532
- Umurhan O. M., 2010, *A&A*, 521, A25
- Umurhan O. M., 2012, *A&A*, 543, A124